A&A 574, A111 (2015)
DOI: 10.1051/0004-6361/201425263

Astronomy & Astrophysics

A forming wide polar-ring galaxy at z ∼ 0.05 in the VST Deep Field of the Fornax cluster⋆

E. Iodice[1], M. Capaccioli[1,2], M. Spavone[1], N. R. Napolitano[1], A. Grado[1], L. Limatola[1], M. Cantiello[3], and P. Schipani[1]

[1] INAF – Osservatorio Astronomico di Capodimonte, via Moiariello 16, 80131 Naples, Italy
e-mail: iodice@na.astro.it
[2] Dipartimento di Fisica, Universitá di Napoli "Federico II", via Cintia 21, 80126 Naples, Italy
[3] INAF – Osservatorio Astronomico di Teramo, via Maggini, 64100 Teramo, Italy

Received 3 November 2014 / Accepted 21 November 2014

ABSTRACT

We present the first deep photometry of what may be a good candidate for a forming polar-ring galaxy at redshift $z \simeq 0.05$. The object FCSS J033710.0-354727 is a background galaxy in the VST Deep Field of the Fornax cluster. The deep exposures combined with the high angular resolution of the OmegaCam at VST allowed us to carry out the first detailed photometric analysis for this system in the g and i bands to derive the galaxy structure and colors. Results show that the central object resembles a disk galaxy, surrounded by a ring-like structure that is twice as extended as the central disk. The warped geometry and bright knots observed along the polar direction, as well as some debris detected on the NW side with colors similar to those of the galaxy, suggest that the polar structure is still forming. We argue that the wide polar ring or disk is the result of the ongoing disruption of a companion galaxy in the potential well of the central object, which is two to three times more massive than the accreting galaxy.

Key words. galaxies: photometry – galaxies: peculiar – galaxies: structure – galaxies: formation – surveys

1. Introduction

Polar-ring or disk galaxies (PRGs) are multi-spin systems. The polar structure consists of dust and gas that rotates in a perpendicular plane with respect to the stars of the central galaxy (see Iodice 2014, for a review). A "second event" is invoked in the formation history of PRGs to explain the decoupling of the angular momentum. Thus, PRGs belong to the group of galaxies best suited for studying the physics of accretion and interaction mechanisms, disk formation, and the dark halo shape. New deep surveys have shown that multi-spin galaxies are quite common at high redshift, and studying these systems at increasing redshift gives fundamental information on the physical processes at work (i.e., merging and accretion) during the formation of galaxies (see Conselice 2014, for a review). There are few studies on PRGs at high redshifts ($z \geq 0.05$), where the dominant component, the central galaxy, is easily visible. Detecting the faint, bluer, and dusty polar structure requires deep imaging, with high spatial resolution. The most distant kinematically confirmed PRG is at $z \sim 0.06$ (Brosch et al. 2010). At higher redshifts ($z \sim 0.06$–1.3), there are only few PRG candidates to be confirmed (Reshetnikov 1997; Reshetnikov & Dettmar 2007). The photometric analysis performed on PRGs at $z \geq 0.05$ shows that in all of them the polar structure has an almost regular ring-like shape, with some clumps of light due to star-forming regions. To date, there is no detailed study of a forming PRG, where the polar structure is still being formed in an intermediate stage, as in the well-studied galaxies NGC 3808B and NGC6286 at $z \sim 0.02$ (Reshetnikov et al. 1996). In the new SDSS-based polar-ring catalog (SPRC) compiled by Moiseev et al. (2011), which reports several new PRG candidates in a wide range of redshift, only two objects appear to be in an ongoing interaction to form a PRG at $z \geq 0.05$ (SPRC199 and SPRC226), but both of them are neither kinematically confirmed nor studied in detail. At $z \sim 0.02$ a forming polar disk is found in the wall between voids, resulting from the slow accretion of gas (Stanonik et al. 2009): the polar structure only consists of neutral hydrogen (it was detected in the HI emission), and the gas density is still too low to form the stellar counterpart. In this paper we present the detailed photometric analysis of the background galaxy FCSS J033710.0-354727 at $z \sim 0.05$, which is a good candidate to be the first forming wide PRG at this redshift.

2. Observations and data reduction

As part of the VST Survey of Elliptical Galaxies in the Southern hemisphere (VEGAS, Capaccioli & Schipani 2011), which is a guaranteed time observation survey performed at the ESO VLT Survey Telescope (VST), we have obtained a mosaic of 1.75×1.59 degrees of the Deep Field of the Fornax cluster, around the cD galaxy NGC 1399. Images were collected in the g and i bands in October 2011. VST is a 2.6 m wide field optical survey telescope, located at Cerro Paranal in Chile. The VST is currently the largest telescope in the world that is specially designed for surveying the sky in visible light; this ESO work-horse is entirely dedicated to visible survey programs. The telescope is an F/5.5 with an alt-azimuth mount, equipped with an active optics system (Schipani et al. 2010, 2012). VST is equipped with the wide-field camera OmegaCam, spanning a 1×1 degree^2 field of view in the optical wavelength range from 0.3 to 1.0 micron (Kuijken 2011). The mean pixel scale is 0.21 arcsec/pixel. The region of maximum overlap of all pointings is around the galaxy NGC 1389, where the total integration time is 3 h in the g band and 1.4 h in the i band. The average seeing is about 1 arcsec.

⋆ This work is based on observations taken at the ESO La Silla Paranal Observatory within the VST GTO Program ID 088.B-4012(A).

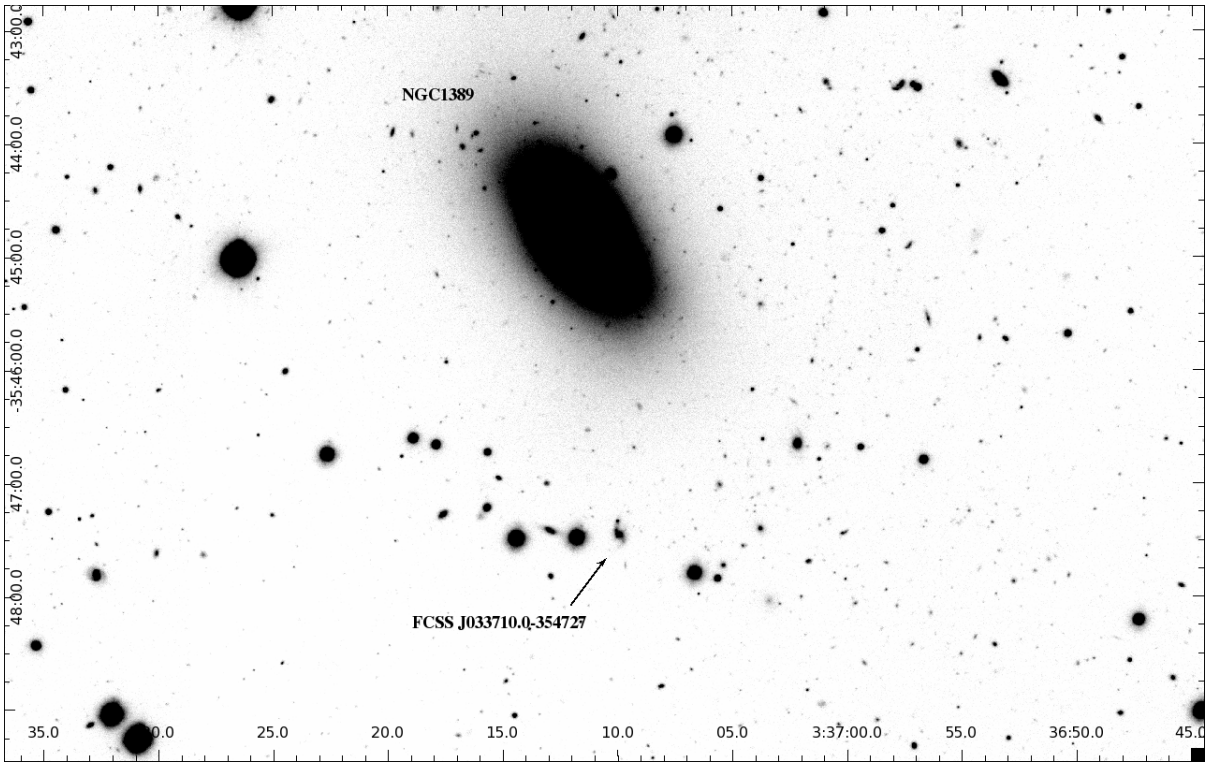

Fig. 1. Field around the bright S0 galaxy NGC 1389 in the g-band VST Deep Field of the Fornax cluster. The arrow locates the background galaxy FCSS J033710.0-354727.

The data were reduced with the *VST-Tube* imaging pipeline (Grado et al. 2012). This provides fully calibrated images from the raw data through the following steps: 1) overscan, bias and flat-field correction; 2) CCD gain equalization and illumination correction; 3) astrometric and photometric calibration, applied before stacking for the final co-added image. For a detailed description of the data reduction procedure see Ripepi et al. (2014). To perform a deep surface photometry of the extended galaxies in the VEGAS survey, the VST-tube pipeline also includes a task to remove the background patterns. This will be described in a forthcoming paper, which is dedicated to the first results of the VEGAS survey (Capaccioli et al., in prep.). Because the studied object covers a very small area (its diameter is $D \lesssim 30$ arcsec, see Sect. 3), the background has been estimated locally in this work, in the regions surrounding the galaxy.

3. Galaxy FCSS J033710.0-354727: morphology and light distribution

The background galaxy FCSS J033710.0-354727 at $z \sim 0.051$ is located south of the bright S0 galaxy NGC 1389 in the Fornax cluster (see Fig. 1). It is characterized by a central component that we named host galaxy (HG) and is surrounded by a warped ring-like structure (see left panels of Figs. 2 and 3). The main properties of FCSS J033710.0-354727 are listed in Table 1. According to Brocca et al. (1997), inside a distance of about five times its diameter, that is $R \leq 200$ kpc (see Table 1), no companion galaxies at similar measured redshift are found around FCSS J033710.0-354727, which could be an isolated object. We analyzed images in the g and i bands to derive the galaxy structure and colors.

Morphology – The VST image of FCSS J033710.0-354727 in g and i bands is shown in the left panels of Figs. 2 and 3.

Table 1. Global properties of FCSS J033710.0-354727.

Parameter	Value	Ref.
Morphological type	Sc peculiar	NED[a]
RA (J2000)	03h37m09.94s	NED
Dec (J2000)	−35d47m27.2s	NED
Helio. radial velocity	15 447 km s^{-1}	NED
Redshift	0.051	FCSS[b]
Distance	206 Mpc	
Scale	1 kpc/arcsec	
Diameters	3.4 × 40 kpc	this work
Magnitudes[c]		this work
m_g	18.59 mag	
m_i	18.03 mag	
M_g	−18.00 mag	
M_i	−18.48 mag	
	Central galaxy:	
m_g	20.47 mag	
m_i	19.90 mag	
M_g	−16.12 mag	
M_i	−16.61 mag	
$g-i$	0.6 mag	
	Polar structure:	
m_g	19.09 mag	
m_i	18.53 mag	
M_g	−17.54 mag	
M_i	−17.99 mag	
$g-i$	0.56 mag	

Notes. [(a)] NASA/IPAC Extragalactic Database. [(b)] The Fornax Spectroscopic Survey (Drinkwater et al. 2000). [(c)] Absolute magnitudes are corrected for both galactic extinction and K-correction, while apparent magnitudes take into account only galactic extinction, see text for details.

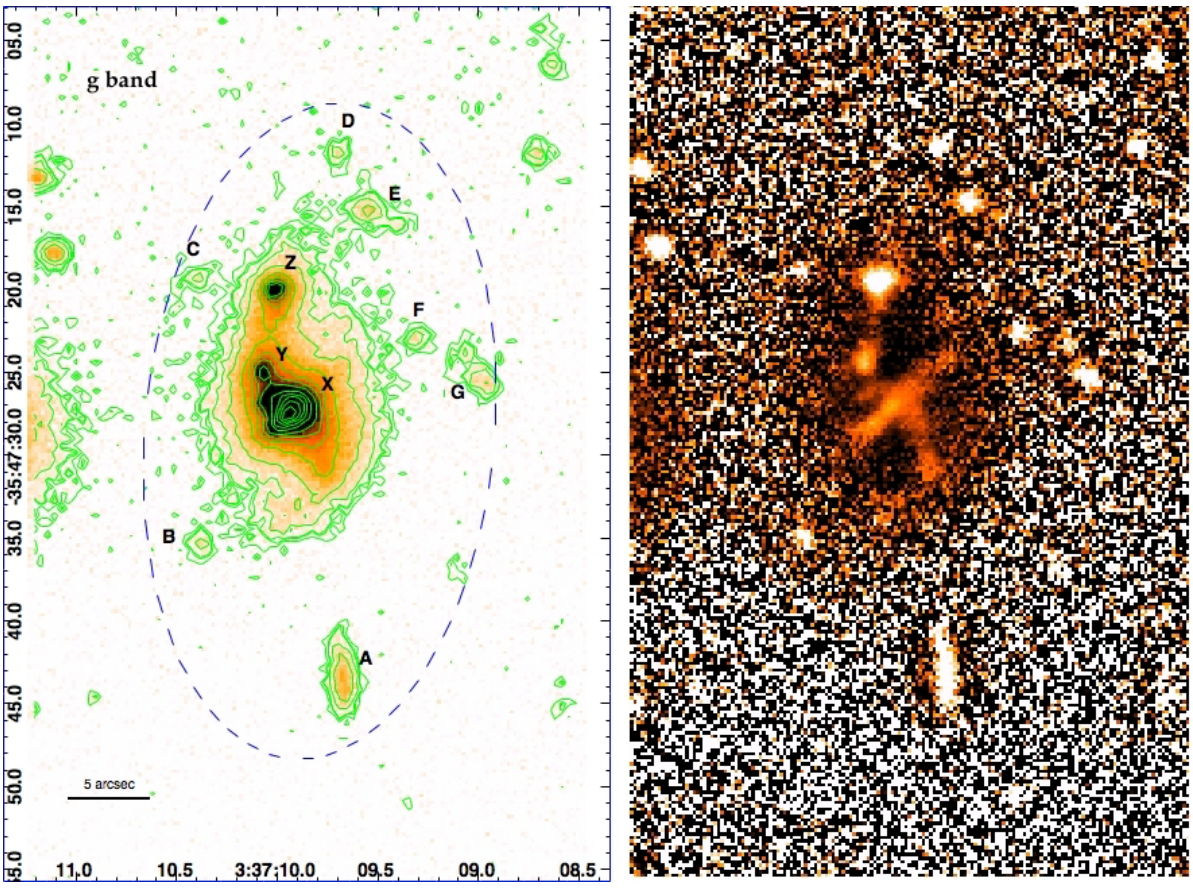

Fig. 2. *Left panel*: VST image of FCSS J033710.0-354727 in g band and the isophote contours (green lines). Labels indicate the center of the galaxy, X, the two bright knots inside the polar structure, Y and Z, and several bright features, from A to G, which are apparently distributed on an elliptical orbit (blue dashed line) around the polar direction. *Right panel*: high-frequency residual images of FCSS J033710.0-354727 in the g band (see Sect. 3 for details). North is up and east is on the left.

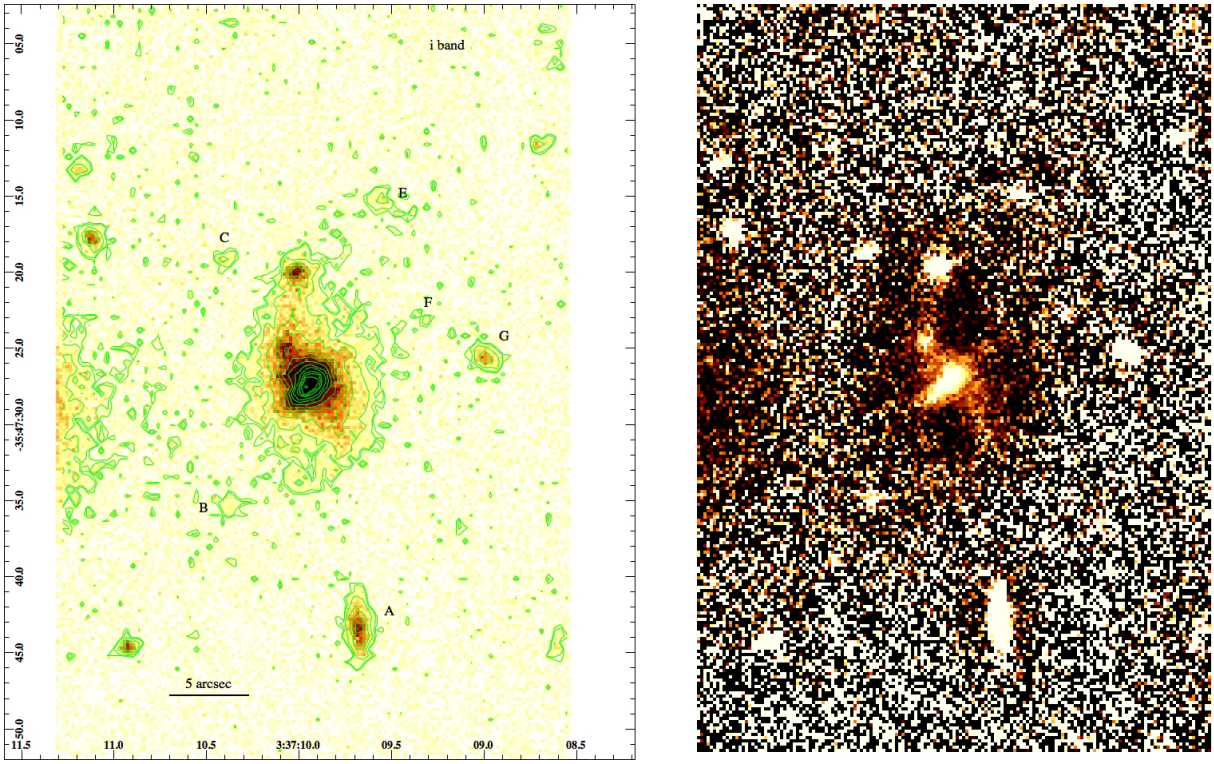

Fig. 3. *Left panel*: VST image of FCSS J033710.0-354727 in i band and the isophote contours (green lines). Labels are the same as in Fig. 1, 2. *Right panel*: high-frequency residual images of FCSS J033710.0-354727 in the i band. North is up and east is on the left.

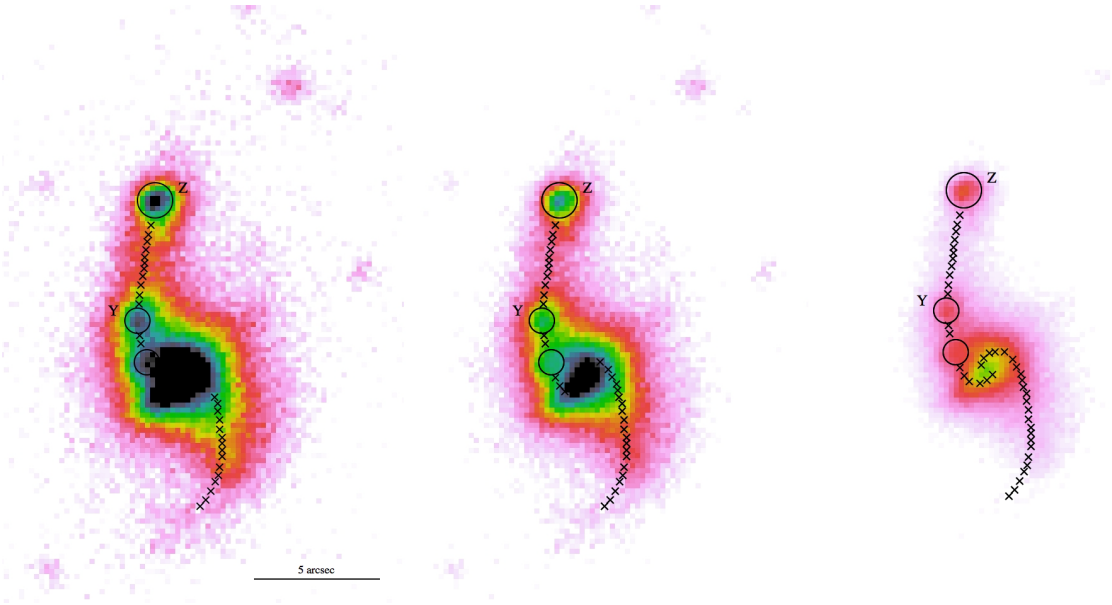

Fig. 4. VST images of FCSS J033710.0-354727 in g band with different contrasts to emphasize the morphology of the galaxy close to center. The highest level increases from left to the right. Labels are the same as in Figs. 1 and 2. The three circles indicates the bright blobs of light along the northern arm of the polar structure. The cross signature in each panel follows the bright path of the polar structure up to the galaxy center (see Sect. 3 for details). North is up and east is on the left.

The center of the galaxy, labeled X, contributes most of the light. Towards the north are two other bright knots, labeled Y and Z, which are inside the polar structure. At larger distances from the galaxy center, we observe several bright features that are apparently distributed on an elliptical orbit around the polar direction, one of this (labeled A) probably is a disk galaxy. None of the above objects have a redshift measurement. We derived the high-frequency residual images of FCSS J033710.0-354727 in the g and i bands (see right panels of Figs. 2 and 3) as the ratio of the original reduced image with a smoothed[1] one, where each original pixel value is replaced with the median value in a rectangular window. The high-frequency residual images show a disk-like structure along the major axis of the central component. The polar structure extends up to the galaxy center, crossing it by tracing an S-shaped pattern. It is characterized by a very bright peak at the end of the northern arm. Figure 4 shows the g-band image of FCSS J033710.0-354727 with different contrast: close to center, the light of the HG is not symmetric and is perturbed by the two arms of the polar structure that are approaching the nucleus. In particular, on the NE side there is a third bright knot, whose light is smeared in the light coming from the central HG. Although the morphology of FCSS J033710.0-354727 could be also similar to that of late-type barred galaxy (in which scenario the central disk would be the bar with loosely wound and highly inclined arms), the qualitative analysis of the structure observed for FCSS J033710.0-354727 described above suggests that this object should be classified as a PRG. The two arms of the polar structure cross the center of the galaxy, they do not start from the edge of the central disk or bar. Moreover, the accreting loop observed toward the galaxy center was also observed in other forming polar rings at lower redshifts, such as ESO 474-G26 (see Fig. 14 of Spavone et al. 2012) and VGS31b (see Fig. 4 of Spavone & Iodice 2013).

Surface photometry – We used the ELLIPSE task in IRAF on the g- and i-band images to perform the isophotal analysis. All the bright features around FCSS J033710.0-354727 were masked, including background objects and bright stars in the field. The azimuthally averaged surface brightness profiles, the position angle (PA), and the ellipticity (ϵ) are shown in Fig. 5. The limits of the surface photometry were derived as the distance from the center where the galaxy light blends into the background level, which was found to be 23 arcsec (~23 kpc) in both g and i band. The limiting magnitudes corresponding to the limiting radii given above are $\mu_g = 29.3 \pm 0.3$ mag arcsec^{-2} for the g band and $\mu_i = 27.7 \pm 0.3$ mag arcsec^{-2} for the i band. The error estimates on the magnitudes take the uncertainties on the photometric calibration (~0.02 mag) and sky subtraction ($\simeq$0.06 ADU in the g band and $\simeq$0.2 ADU in the i band) into account.

The azimuthally averaged surface brightness profiles in the g and i bands (see Fig. 5, left panel) are quite smooth on the whole range of radii, except for the two peaks of light at $R \sim 3.5$ arcsec (~3.5 kpc) and $R \sim 7$ arcsec (~7 kpc), which correspond to the bright knots labeled Y and Z in Fig. 2 (left panel). The PA and ellipticity profiles (Fig. 5, right panels) show an abrupt change in the shape at $R \leq 1.69$ arcsec (~1.7 kpc): the isophotes in the left panel of Fig. 2 show that this radius corresponds to the transition from the HG to the polar ring (PR) and set a constraint on the radial extent of the two components that is $R_{\rm HG} \sim 2$ kpc and $R_{\rm PR} \sim 20$ kpc. For $R \geq 1.69$ arcsec, that is, along the polar structure major axis, and up to $R \sim 20$ arcsec (~1.7−20 kpc), a strong twisting is observed as the PA varies by about 70°. In this range of radii, the flattening increases from 0.1 to 0.4. We obtained the 2D model from the fit of the isophotes[2] in the g band and subtracted it from the original image. The 2D residual is shown in Fig. 6. As already found from the high-frequency residual image (right panels of Figs. 2 and 3) and from the high-level contrast in the g band (see Fig. 4), an S-shaped structure is clearly detectable in the polar direction. It extends from north to south and crosses the galaxy center, drawing a spiral loop across the

[1] We used the IRAF task FMEDIAN to smooth the original reduced image by adopting a box of 25 × 25 pixels.

[2] The 2D model of the fitted isophotes was obtained by using the IRAF task BMODEL.

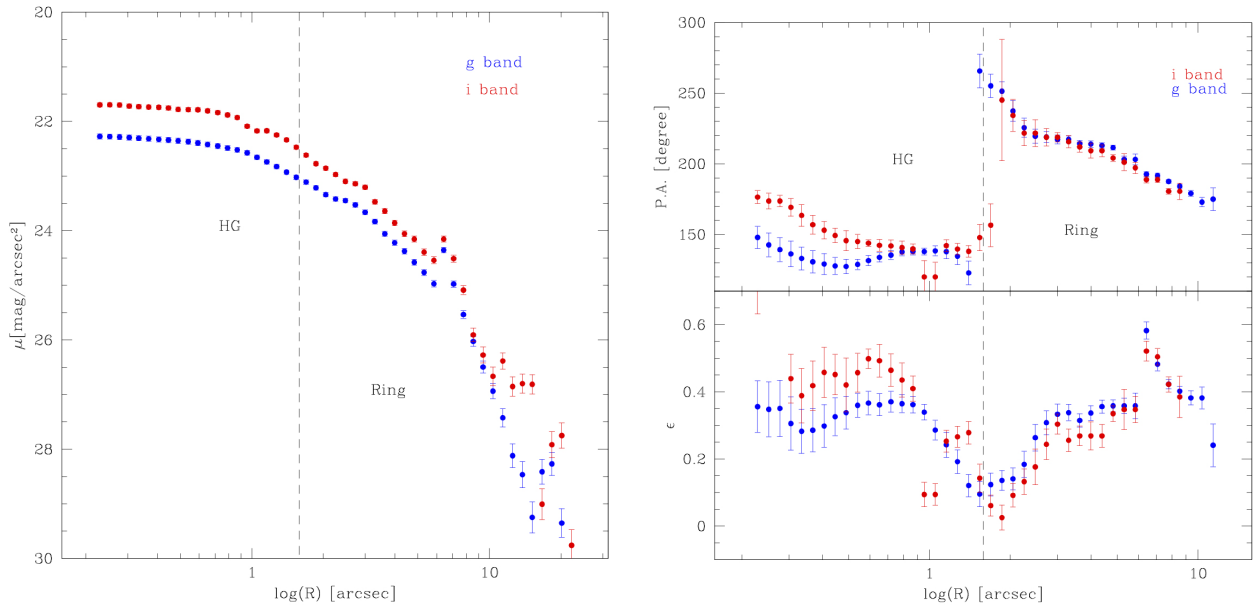

Fig. 5. *Left panel*: azimuthally averaged surface brightness profiles as a function of log(R) derived from the isophote fit. R is the isophote major axis. Data are for the g-band (blue dots) and i-band image (red dots). The dashed line delimits the regions where the main components (HG and polar ring) of the galaxy structure are located. *Right panel*: average profiles of PA (*top panel*) and ellipticity (*bottom panel*) as a function of log(R).

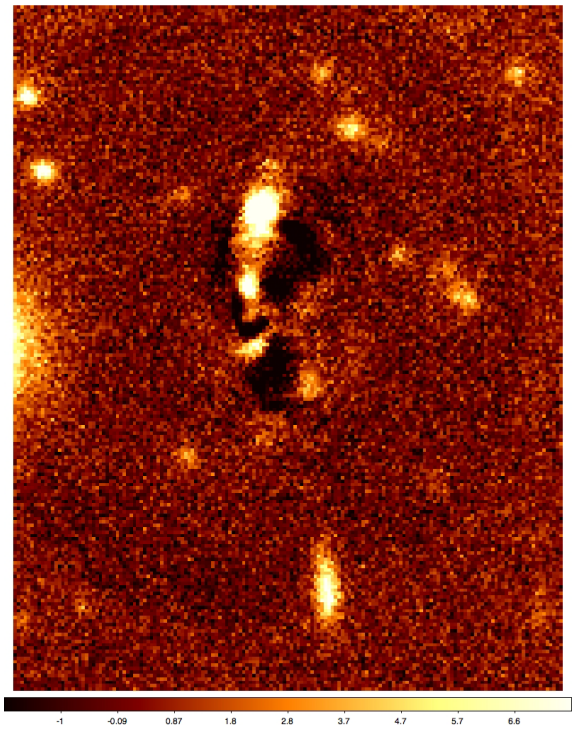

Fig. 6. Residual image obtained by subtracting the 2D model derived from the fit of isophotes from the original image in the g band. The image size is 34×42 arcsec (~34×42 kpc).

nucleus, and is characterized by two bright knots in the northern arm.

We derived the integrated magnitudes in the g and i bands inside the elliptical aperture that correspond to the last fitted isophote for the whole galaxy and for the two components (HG and polar structure). Values were corrected for the extinction within the Milky Way by using the absorption coefficient $A_g = 0.035$ and $A_i = 0.018$ derived according to Schlegel et al. (1998). The K-correction was applied to the absolute magnitudes, where the correction factors in g and i band are $K_g = 0.02$ and $K_i = -0.06$ (Chilingarian et al. 2010; Chilingarian & Zolotukhin 2012).

Light profiles – We extracted the light profiles along the major axis of the two main components in FCSS J033710.0-354727 (see Fig. 7). The PAs of these directions are defined from the fit of the isophotes (see right panels of Fig. 5). Because of the S-shape of the polar structure, which generates the observed twisting, we adopted the two directions at PA = 8° and PA = 30° that intersect the two bright knots Y and Z.

The surface brightness of the central component extends up to about 8 arcsec (~8 kpc). It is not symmetric with respect to the center of the galaxy. For $R \geq 2$ arcsec, the NW part of the light profile is brighter than the SE part. We performed a least-squares fit of the HG light profiles (NW and SE sides) by using an exponential law given by

$$\mu(R) = \mu_0 + 1.086 \times R/r_h,$$

where R is the galactocentric distance, μ_0 and r_h are the central surface brightness and scale length of the disk. The best-fit values for the structural parameters found for the NW profile are $\mu_0^{NW} = 22.21 \pm 0.05$ mag/arcsec^2 and $r_h^{NW} = 1.89 \pm 0.04$ arcsec, and for the SE profile they are $\mu_0^{SE} = 22.07 \pm 0.10$ mag/arcsec^2 and $r_h^{SE} = 1.41 \pm 0.05$ arcsec. For $R \leq 2$ arcsec there is an excess of light of about 0.2 mag, which is quite symmetric with respect to the center, contrary to what is observed at larger radii. This feature could be related to a small bulge.

Along the polar structure the surface brightness is twice as extended as that along the HG, out to $R \sim 20$ arcsec (~20 kpc). The peak of light corresponding to Z is less than one magnitude fainter than the galaxy center.

Integrated magnitudes and colors – Figure 8 shows the isophotal $g - i$ color profile. The central spheroid for $R \leq 1.6$ arcsec is redder than the polar structure, which on average has a color of $g - i \sim 0.58$ mag. For $R > 1.6$ arcsec, the color profile has a steep gradient toward bluer colors, reaching a value of $g - i \sim 0.2$ mag at $R \sim 10$ arcsec.

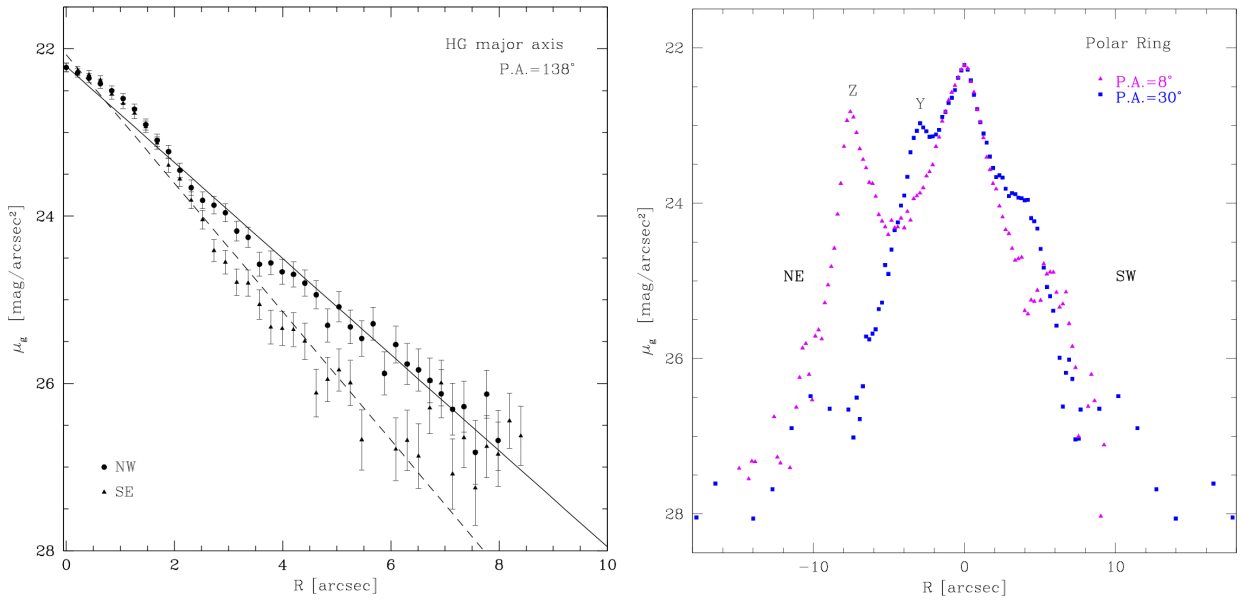

Fig. 7. *Left panel*: folded light profiles in the g band along the major axis of the central spheroid. The continuos and dashed lines are the results of the exponential fits to the light distribution for the NW (circles) and SE (triangles) sides (see Sect. 3 for details). *Right panel*: light profiles in the g band along the polar structure. The two directions at PA = 8° and PA = 30° are chosen to intersect the two bright knots Y and Z, observed in the northern arm (see also Fig. 2 left panel).

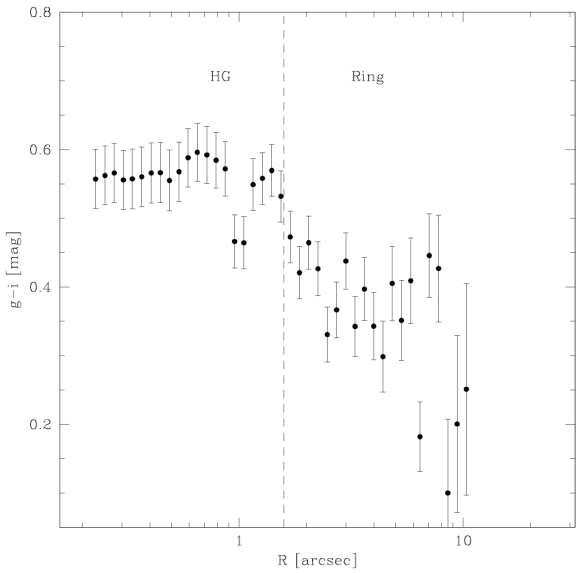

Fig. 8. Azimuthally averaged $g - i$ color profile as function of log(R) derived from the isophote fit. R is the isophote major axis. The dashed line delimits the regions where the main components (HG and polar ring) of the galaxy structure are located.

We derived the integrated magnitudes and $(g - i)$ colors in circular apertures[3] of the center of galaxy, the two bright knots Y and Z, and of all the bright objects around the galaxy (see left panel of Fig. 2). Values are listed in Table 2. As already shown from the light profiles, the bright knot Z on the NE side is only 0.5 mag fainter than the galaxy center. The center of the galaxy is redder than the two knots on the north side of the polar structure and it has $(g - i) = 0.55$ mag. The closest knot to the central spheroid, labeled Y, has $(g - i) = 0.35$ mag, while the outer and more luminous knot Z of the polar structure has a bluer color $(g - i) = 0.13$ mag. The integrated colors of the bright objects observed around FCSS J033710.0-354727 have a bimodal distribution. The galaxy labeled A and the two bright objects B and G have $(g - i) \geq 1$ mag, while for all the other sources we measured $0.3 \leq (g - i) \leq 1$ mag. In particular, the objects D, E and F, located in the NW region of FCSS J033710.0-354727, have $(g - i)$ colors comparable with the range of colors derived for the polar structure. From the $g - i$ colors we estimated the mass-to-light ratio (M/L) for the central galaxy and the polar structure with the stellar population synthesis model GISSEL[4] (Bruzual & Charlot 2003) to constrain the total stellar mass for each component. Assuming a simple stellar population with solar metallicity, the models predict an $M/L \sim 0.6$ for the central galaxy and for the polar structure an $M/L \sim 0.3$–0.6. From the total magnitudes in the g band (see Table 2), the stellar mass in the HG is $M^{\rm HG} \sim 2\times 10^8\ M_\odot$, in the polar structure it is $M^{\rm PR} \sim 1\times 10^8\ M_\odot$. These should be considered as lower limits for the total baryonic mass, since we lack information about the gas content in this galaxy, which is typically high in PRGs, from 10^8 to $10^{10}\ M_\odot$, (see Iodice 2014, and references therein). In particular, since the gas is commonly associated with the polar structure, the baryoinc mass of this component in FCSS J033710.0-354727 could be even higher. Thus, we found 3:1 to 2:1 as lower limits for the stellar mass ratio between the central disk and the polar structure.

4. Results: ongoing formation of a wide polar-ring or disk

The deep exposures in the g and i bands, combined with the high angular resolution of the OmegaCAM at VST, allow us to carry out the first detailed photometric analysis of the background galaxy FCSS J033710.0-354727 at $z \sim 0.05$ in the field of the Fornax cluster.

[3] The radius of each circular aperture is set to include twice the peak of light.

[4] Galaxies Isochrone Synthesis Spectral Evolution Library.

Table 2. Integrated magnitudes and colors for regions in FCSS J033710.0-354727 in circular apertures.

Region	α	δ	R	m_g	m_i	$g-i$
	[s]	[arcsec]	[arcsec]	[mag]	[mag]	[mag]
(1)	(2)	(3)	(4)	(5)	(6)	(7)
X	09.93	27.15	1.05	21.14 ± 0.02	20.61 ± 0.02	0.53 ± 0.04
Y	10.07	24.71	1.05	21.98 ± 0.03	21.63 ± 0.03	0.35 ± 0.06
Z	09.94	20.17	1.47	21.64 ± 0.02	21.53 ± 0.03	0.11 ± 0.05
A	09.67	43.39	2.31	22.57 ± 0.04	21.30 ± 0.02	1.27 ± 0.05
B	10.38	35.53	1.89	23.68 ± 0.07	22.65 ± 0.06	1.03 ± 0.13
C	10.41	19.29	1.47	23.95 ± 0.08	23.01 ± 0.07	0.94 ± 0.15
D	09.69	11.61	1.89	23.75 ± 0.08	23.49 ± 0.12	0.26 ± 0.2
E	09.55	15.28	1.89	23.16 ± 0.06	22.48 ± 0.06	0.68 ± 0.12
F	09.30	23.13	1.47	24.00 ± 0.08	23.41 ± 0.10	0.60 ± 0.2
G	09.00	24.79	2.31	23.00 ± 0.05	21.93 ± 0.04	1.07 ± 0.09

Notes. Column 1: region of FCSS J033710.0-354727 labeled in Fig. 2. Columns 2 and 3: celestial coordinates of the center of each circular aperture, see left panel of Fig. 2 for reference. Column 4: radius of the circular aperture in arcsec. Columns 5 and 6: integrated magnitudes in the g and i bands corrected for galactic extinction. Column 7: integrated $g-i$ color.

The main results (see Sect. 3) show that

- the system is characterized by a central component, surrounded by a warped ring-like structure (see Figs. 2 and 4.);
- the central component is a disk with an exponential surface brightness profile;
- the polar structure is twice as extended as the central disk. It crosses the galaxy center along the north-south direction, drawing a spiral loop across the nucleus. It is characterized by two bright knots, one of them (Z) with a luminosity almost similar to that of the galaxy center;
- the central galaxy is redder ($g-i \sim 0.55$ mag) than the polar structure ($g-i \sim 0.13$–0.4 mag);
- the integrated colors of the bright objects detected around FCSS J033710.0-354727 have a bimodal distribution. Only those located on the NW region have ($g-i$) colors comparable with those derived for the polar structure (see Table 2), thus they can be considered as features related to the galaxy.

The new observations and analysis are in favor of classifying this galaxy as a PRG. In particular, the whole morphology and the large polar extension suggest that this system can be considered to be a good candidate for a wide polar-ring or disk galaxy, similar to NGC 4650A (Iodice et al. 2002). In FCSS J033710.0-354727, the warped geometry of the polar structure and the bright knots along its light distribution, as well as the debris observed on the NW side with similar colors, suggests that the polar structure is still forming. Given the high luminosity, comparable with that of the galaxy center, the two knots Y and Z (see Fig. 2) could be the remnants of a companion galaxy that is disrupting in the potential of the central disk, which is two to three times more massive than the accreting object. This mechanism, that is, the tidal accretion of material from outside, is one of the possible formation scenarios proposed for PRGs (see Combes 2014, as review). In this framework, taking into account the low stellar mass ratio between the central disk and the polar structure (3:1–2:1) and the high inclination of the accreting material, numerical simulations (Bournaud & Combes 2003) are able to form a massive and extended polar-ring or disk, as observed in FCSS J033710.0-354727. From comparing the snapshots of the simulation with the observed morphology for FCSS J033710.0-354727, we suggest that this gravitational interaction is still ongoing, which means that we witness the intermediate stage of the PRG formation at an epoch of about 2 Gyr.

Alternatively, FCSS J033710.0-354727 might also be a post-merger system, where two big galaxies have already coalesced into a single system, with two tidal tails around it and an accumulation of mass at the tip of the northern tail, similar to NGC 7252 (Hibbard & Mihos 1995). One observational fact in favor of the tidal accretion process instead of the major merger is the large mass of the bright knot Z, which is not typically found in tidal tail, and the S-shape feature that connects the outer parts of the polar structure to the galaxy center (see right panel of Fig. 2), which is more similar to an accreting loop than to tidal tail remnants. Kinematic measurements are needed, not only to confirm FCSS J033710.0-354727 as a PRG, but also to distinguish between the two formation mechanisms. In particular, if this galaxy is the remnant of a major merger between two disk galaxies, we expect to find the central object to be dominated by random motions (Bournaud & Combes 2003).

In conclusion, FCSS J033710.0-354727 is a peculiar system at $z \sim 0.05$ resulting from the interaction of two massive galaxies, which could form a wide polar-ring or disk galaxy. As discussed in Sect. 1, the few PRGs studied at $z \geq 0.05$ show a well-formed polar structure, without any tail or ripple that would suggest an ongoing interaction event. The main result of this work is that to date, FCSS J033710.0-354727 is the most distant PRGs in formation for which a detailed photometric analysis has been performed: the intermediate stage captured for this object allowed us to derive the important constraint on the mass ratio of the two interacting galaxies, which is hard to estimate, or quite uncertain, in a final remnant galaxy.

Acknowledgements. We are very grateful to the anonymous referee for his or her comments and suggestions that helped us to improve and clarify our work. This work was supported by the PRIN-INAF "Galaxy Evolution with the VLT Survey Telescope (VST)" (PI A. Grado). M. Cantiello acknowledges support from PO FSE Abruzzo 2007-2013 (PO 2012/2013).

References

Bournaud, F., & Combes, F. 2003, A&A, 401, 817
Brocca, C., Bettoni, D., & Galletta, G. 1997, A&A, 326, 907
Brosch, N., Kniazev, A. Y., Moiseev, A., & Pustilnik, S. A. 2010, MNRAS, 401, 2067
Bruzual, G., & Charlot, S. 2003, MNRAS, 344, 1000
Capaccioli, M., & Schipani, P. 2011, The Messenger, 146, 2
Chilingarian, I. V., & Zolotukhin, I. Y. 2012, MNRAS, 419, 1727

Chilingarian, I. V., Melchior, A.-L., & Zolotukhin, I. Y. 2010, MNRAS, 405, 1409
Combes, F. 2014, in Multi-Spin Galaxies, eds. E. Iodice, & E. M. Corsini, ASP Conf. Ser. 486, 207
Conselice, C. J. 2014, in Multi-Spin Galaxies, eds. E. Iodice, & E. M. Corsini, ASP Conf. Ser. 486, 85
Drinkwater, M. J., Phillipps, S., Jones, J. B., et al. 2000, A&A, 355, 900
Grado, A., Capaccioli, M., Limatola, L., & Getman, F. 2012, Mem. Soc. Astron. It. Suppl., 19, 362
Hibbard, J. E., & Mihos, J. C. 1995, AJ, 110, 140
Iodice, E. 2014, in ASP Conf. Ser. 486, eds. E. Iodice, & E. M. Corsini, 39
Iodice, E., Arnaboldi, M., De Lucia, G., et al. 2002, AJ, 123, 195
Kuijken, K. 2011, The Messenger, 146, 8
Moiseev, A. V., Smirnova, K. I., Smirnova, A. A., & Reshetnikov, V. P. 2011, MNRAS, 418, 244
Reshetnikov, V. P. 1997, A&A, 321, 749
Reshetnikov, V. P., & Dettmar, R.-J. 2007, Astron. Lett., 33, 222
Reshetnikov, V. P., Hagen-Thorn, V. A., & Yakovleva, V. A. 1996, A&A, 314, 729
Ripepi, V., Cignoni, M., Tosi, M., et al. 2014, MNRAS, 442, 1897
Schipani, P., D'Orsi, S., Ferragina, L., et al. 2010, Appl. Opt., 49, 1234
Schipani, P., Noethe, L., Arcidiacono, C., et al. 2012, J. Opt. Soc. Am. A, 29, 1359
Schlegel, D. J., Finkbeiner, D. P., & Davis, M. 1998, ApJ, 500, 525
Spavone, M., & Iodice, E. 2013, MNRAS, 434, 3310
Spavone, M., Iodice, E., Bettoni, D., et al. 2012, MNRAS, 426, 2003
Stanonik, K., Platen, E., Aragón-Calvo, M. A., et al. 2009, ApJ, 696, L6